Japanese Journal of Comprehensive Rehabilitation Science (2012)

Original Article

Development of an integration circuit to measure pulsed magnetic field: evaluation of its usefulness by comparing measured with theoretical magnetic field structure

Shin-Ichi Izumi, MD, PhD,[1,2] Yutaka Oouchida, PhD,[2] Taishi Okita, PhD,[3] Eizaburo Suzuki, RPT, MS,[2] Toshihiko Abe, PhD,[4] Ryoichi Nagatomi, MD, PhD,[5] Nobukazu Nakasato, MD, PhD,[6] Toshiyuki Takagi, PhD[3]

[1]Department of Physical Medicine and Rehabilitation, Tohoku University Graduate School of Biomedical Engineering, Sendai, Miyagi, Japan
[2]Department of Physical Medicine and Rehabilitation, Tohoku University Graduate School of Medicine, Sendai, Miyagi, Japan
[3]Institute of Fluid Science, Tohoku University, Sendai, Miyagi, Japan
[4]IFG Co.,Ltd, Sendai, Miyagi, Japan
[5]Laboratory of Health and Sports Science, Tohoku University Graduate School of Biomedical Engineering, Sendai, Miyagi, Japan
[6]Department of Epileptology, Tohoku University Graduate School of Medicine, Sendai, Miyagi, Japan

ABSTRACT

Izumi S, Oouchida Y, Okita T, Suzuki E, Abe T, Nagatomi R, Nakasato N, Takagi T. Development of an integration circuit to measure pulsed magnetic field: evaluation of its usefulness by comparing measured with theoretical magnetic field structure. Jpn J Compr Rehabil Sci 2012; 3: 42–50.

Objective: To develop a search coil with a capacity-resistor (CR) integration circuit for instantaneous measurement of a pulsed magnetic field, and to compare the magnetic field structure measured by the novel device with the theoretical values.

Methods: The integration circuit consists of a capacitor and a resistor connected in series, and generates a voltage output across the capacitor. For magnetic field measurement, we selected capacitance × resistance = 4 ms. Using the search coil and CR integration circuit, we measured the magnetic flux density generated by a circular coil, over a range of magnetic flux densities (0.1 to 1.4 T) and pulse widths (0.1 to 0.6 ms). We also obtained the corresponding magnetic fields by numerical integration of the electromotive force induced in the search coil. Then we measured the distribution of magnetic flux densities generated by a commercial figure-of-eight coil commonly used in transcranial magnetic stimulation (TMS), and compared the results with the magnetic field derived from model calculation.

Results: The values measured by the CR circuit and the values obtained by numerical integration showed good agreement ($R^2 = 0.9993$). At 100% output from the stimulator, the peak magnetic flux density of the horizontal and vertical magnetic fields at a distance 10-30 mm from the figure-of-eight coil surface was 0.2 to 0.5 T. The measured magnetic field showed less focalization when compared with the values obtained from model calculation.

Conclusions: We identified the appropriate CR combination for the integration circuit used to measure a pulsed magnetic field. This device would be useful for quantitative analysis of TMS-induced effects on cortical function.

Key words: transcranial magnetic stimulation, magnetic field structure, figure-of-eight coil, integration circuit, teslameter, magnetic flux density

Correspondence: Shin-Ichi Izumi, MD, PhD
Professor and Chairman, Department of Physical Medicine and Rehabilitation
Tohoku University Graduate School of Biomedical Engineering, 2−1 Seiryo-cho, Aoba-ku, Sendai, Miyagi 980-8575, Japan
E-mail: izumis@bme.tohoku.ac.jp

Accepted: June3, 2012
This research was supported by the Program for Promotion of Fundamental Studies in Health Sciences of the National Institute of Biomedical Innovation, NIBIO for the fiscal year 2006–2008 (Project ID 06−32). No benefits in any form have been or will be received from any commercial party related directly or indirectly to the subject of this manuscript.

Introduction

Transcranial magnetic stimulation (TMS) noninvasively excites neurons in the cerebral cortex by inducing weak electric currents (eddy currents) [1, 2]. Repetitive TMS (rTMS) has recently attracted considerable attention as an effective method to induce plastic changes in the central nervous system. For example, rTMS has been applied for the restoration of motor function following hemiplegia [3–7] and modulation of cognitive function [8–11].

A figure-of-eight (FOE) coil is widely used for medical purposes [12, 13]. The FOE coil is composed of two loops approximately 70 mm in diameter, through which an electric current flows in opposite directions to produce monophasic or biphasic pulsed stimulation. Although the electric field properties of commercial FOE coils used in TMS have been reported [14], the actual eddy currents induced in the human brain have not been measured. Furthermore these currents are difficult to estimate because of the complicated brain structure and insufficient information about the electromagnetic properties, such as conductivity and permittivity, of the human brain.

While actual eddy currents cannot be measured, it is essential to know the electromagnetic characteristics such as the magnetic field intensity of individual TMS coils for quality control of TMS studies. Previously we have found that the coefficient of variation for the pulsed magnetic field intensity measured by commercially available gauss meters for static or alternating magnetic field was approximately 20% (unpublished data). The reason for this large variability is probably because commercial gauss meters are not constructed to measure pulsed magnetic fields with durations around 0.2 ms, which is the usual specification for a commercial TMS device.

Although pulsed magnetic field intensity can be estimated by numerical integration of the electromotive force induced in the search coil, the calculation takes time and effort. Thus we aimed to develop a search coil with a capacitor-resistor (CR) integration circuit to measure the pulsed magnetic field instantaneously. The CR integration circuit, in which the capacitor and resistor are connected in series, generates an output across the capacitor that approximates the numerical integration when the time constant (capacitance x resistance) is adequately larger than the pulse width. We examined the accuracy of the novel instrument by comparing the measured results with those obtained by numerical integration of the electromotive force, and demonstrated its usefulness by comparing the measured and theoretical magnetic field structure induced by a commercially available FOE coil.

Methods

1. Development of an instrument to measure pulsed magnetic field intensity

When a magnetic pulse passes through a search coil, a voltage V is induced that can be expressed by equation (1).

$$V = nS\frac{dB}{dt} \tag{1}$$

where n is the turn number of the search coil, S is the surface area of the coil, B is the magnetic flux density, and t is time.

To express the magnetic flux density B, equation (2) is derived by integration of equation (1).

$$B=\frac{1}{nS}\int Vdt \tag{2}$$

The strength of the magnetic field can be calculated theoretically from (2) by numerical integration of the induced V. This calculation, however, is fairly time-consuming because of the large amount of data, and thus is not applicable to real-time measurements. In order to avoid such complicated numerical integration, the time integration term of equation (2) is replaced by a CR integration circuit (Fig. 1). In this circuit, a resistor with resistance R and a capacitor with capacitance C are connected to the search coil. When the search coil generates a voltage V, and a current I flows in R for a time T, then the stored electric charge Q in the capacitor is:

$$Q = CV_c(T) = \int_0^T I(t)\,dt = \int_0^T \frac{V(t)-V_c(t)}{R}\,dt$$

$$CRV_c(T) \cong \int_0^T V(t)\,dt$$

where V_c is the charge voltage of the capacitor.

In this equation, we assume that CR >> T, and $V_c(0) = 0$.

Since the time integration in equation (2) has been replaced by the time constant CR, B is calculated by the simple equation (3).

$$B = \frac{1}{nS}V_cCR \tag{3}$$

Since equation (3) is so simple and there is no criterion for the values of C and R, it is important to select appropriate C and R values for practical measurements of B. Thus, we investigated the relationship between CR values and CR integral magnetic flux density.

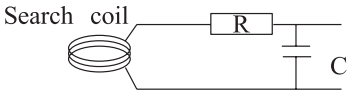

Figure 1. Schematic representation of the CR integration circuit with a search coil.
The capacitor (C) and resistor (R) are connected in series. The output of the circuit is voltage across the capacitor. The search coil is placed in the magnetic field to be measured.

A pulsed magnetic field with a pulse width of 0.17 ms was generated by a custom-made circular coil, and measured using the search coil used in the present study. The search coil was positioned coaxially just above the excitation coil. Numerical integration showed a magnetic flux density amplitude of 0.591 T. As the induced V is low (around 1 V), we selected R lower than 5 kΩ, and measured its resistance up to 4 digits. In addition, we used a ceramic capacitor with a high Q value and measured its capacitance up to 4 digits at 1 kHz. We then set up a CR integration Gauss meter using these criteria. CR integration was performed at constant capacitance (9.705 μF at 1 kHz alternating current) and various resistances ranging from 30 to 2201 Ω. Five measurements for each resistance value were made, and the mean and standard deviation were calculated.

Based on experimental results as shown below (1. Relationship between CR values and CR integral magnetic flux density), we selected CR = 4 ms, which is twenty times longer than the pulse width of 0.2 ms. Another important factor is the size of the search coil because there is an inverse relation between spatial resolution and output voltage. In the present study, we designed n = 10 turns of copper wire (0.3 mm in diameter) and S = 0.2826 cm^2 (6 mm in diameter). We measured the magnetic flux density at the center of various circular coils with pulse widths ranging from 0.1 to 0.6 ms, changing the applied voltage from 400 to 2000 V. The axis of the search coil was oriented parallel to the coil being examined. Magnetic flux densities measured by the CR integration circuit and those obtained by numerical integration of the induced V were compared.

2. Measurement of pulsed magnetic field generated from a FOE coil

We measured pulsed magnetic flux density amplitudes generated by a commercially available 70-mm FOE coil (9925-00, Magstim, Carmarthenshire, UK) and a stimulator (MRS 1000/50, Magstim).

The handle of the FOE coil was held horizontally with its flat side upward by a fastening device. The center of the FOE coil surface was the origin of the x, y and z coordiantes (0, 0, 0). The x-axis was the long axis of the FOE coil; the y-axis was perpendicular to the x-axis; and the z-axis was the vertical axis. By moving the search coil by 5-mm increments in the x- and y-directions and 10-mm in the z-direction in a 3-D system, we measured the magnetic flux densities at a total of 1575 sites (25×21×3) with stimulation intensities at 50% and 100% of the stimulator output (Fig. 2). To measure magnetic flux densities in the direction of the x-(B_x) and z-coordinates (B_z), the axis of the search coil was oriented parallel to the respective coordinate. Five measurements were taken and averaged at each site.

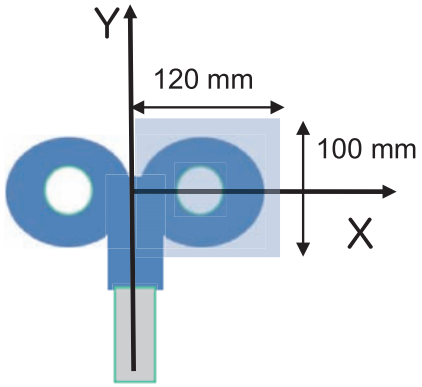

Figure 2. Area of measurement of the pulsed magnetic field generated by the FOE coil.
The origin of the coordinates is set at the center of the coil on the side in contact with the head. The x-axis is the long axis of the figure-of-8, and the y-axis is perpendicular to the x-axis. The square shaded area (120×100 mm) indicates the measurement area in the x-y plane. By moving the search coil by 5-mm increments in the x- and y-directions and 10-mm in the z-direction in a 3-D coordinate system, we measured magnetic flux densities at a total of 1575 sites (25×21×3).

3. Numerical calculation of magnetic flux density

We numerically calculated the spatial distribution of the magnetic flux density, using the FOE coil model. As shown in Fig. 3, the model uses a pair of current loops with 9 turns each [15] and center at A (x_0, 0, 0) and B ($-x_0$, 0, 0) on the x-axis. The outermost loops contact each other at the coordinate origin O. For convenience, the loops are referred to as $C_j^{\pm}$ (j=1, 2, …, 9), where j indicates loop number, and ± represents positive and negative regions of the x-axis. The electric current in C_j^{+} flows in the opposite direction to that in C_j^{-} for all j. The loops are excited by an alternating electric current, $I=I_0e^{-i\omega t}$, where I_0 is the peak current, and $\omega=2\pi f$ is the angular frequency. In this study, we focus on the field distribution near the coil where the radiation effect is negligible, so that the electromagnetic fields can be calculated simply in an electrostatic manner. The nontrivial components of the vector potentials for the FOE coil are given by

$$A_x=\sum_{j=1}^{9}(A_{x,j}^{+}+A_{x,j}^{-}) \tag{4}$$

$$A_y=\sum_{j=1}^{9}(A_{y,j}^{+}+A_{y,j}^{-}) \tag{5}$$

where

$$A_{x,j}^{\pm}=\mp\frac{\mu_0 I a_j}{4\pi}\int_0^{2\pi}\frac{\cos\theta}{\left[a_j^2+(x\mp x_0)^2+y^2+z^2-2a_j\sqrt{(x\mp x_0)^2+y^2}\cos\theta\right]^{1/2}}\frac{y}{\sqrt{(x\mp x_0)^2+y^2}}d\theta \tag{6}$$

$$A_{y,j}^{\pm}=\pm\frac{\mu_0 I a_j}{4\pi}\int_0^{2\pi}\frac{\cos\theta}{\left[a_j^2+(x\mp x_0)^2+y^2+z^2-2a_j\sqrt{(x\mp x_0)^2+y^2}\cos\theta\right]^{1/2}}\frac{x\pm x0}{\sqrt{(x\mp x_0)^2+y^2}}d\theta \tag{7}$$

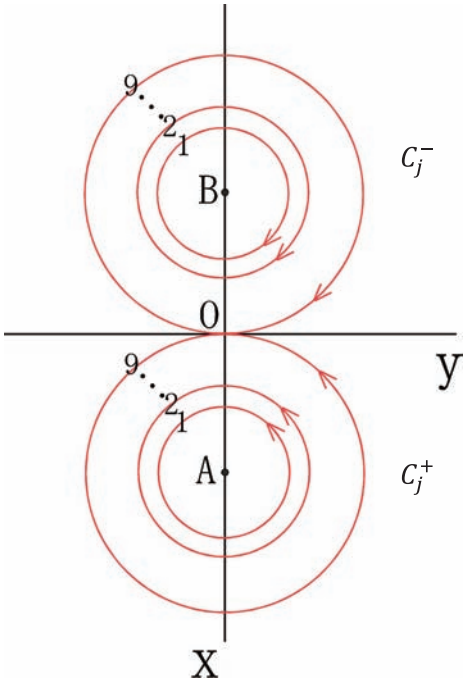

Figure 3. Current flow of the concentric loops.
The model uses a pair of current loops with 9 turns, the same number of turns as a commercially available FOE coil. $C_j^{\pm}$, current at the j-th turn.

and a_j is the radius of the j-th loop $C_j^{\pm}$. The magnetic flux density can therefore be obtained by calculating the curl of the vector potential as described previously [16].

$$B_x = (\nabla \times \vec{A})_x = \frac{\partial A_y}{\partial z} \quad (8)$$

$$B_y = (\nabla \times \vec{A})_y = \frac{\partial A_x}{\partial z} \quad (9)$$

$$B_z = (\nabla \times \vec{A})_z = \frac{\partial A_y}{\partial z} - \frac{\partial A_x}{\partial y} \quad (10)$$

Figure 4 shows a lateral view of one wing of the FOE coil and the analysis planes 1 (z＝10 mm), 2 (z＝20 mm), and 3 (z＝30 mm). The size of the FOE coil (inner radius, 26 mm; outer radius, 44 mm; wire width, 1 mm; wire height, 7 mm) was based on the data from the literature [15]. The thickness of the FOE-coil including the plastic chassis was 30 mm. In this model the coil wire was located midway between the surfaces of the plastic chassis.

The magnetic flux densities B_x in the analysis planes 1, 2, and 3 were calculated as indicated above. Then, the theoretical values of the magnetic flux density were compared with the measured values.

Results

1. Relationship between CR values and CR integral magnetic flux density

As shown in Table 1, the larger the CR values, the nearer the CR integration values approached the value of numerical integration. However, the standard deviation increased as CR became larger (5.99, 11.58, and 21.36 ms). Good agreement in magnetic flux density was obtained between the value obtained from numerical integration (0.591 T) and the values measured using the CR integration circuit at CR values of 4 to 6 ms. However, the standard deviation of CR integration was smaller for the CR value of 4.15 ms than for 5.99 ms. Thus, we selected CR＝4 ms.

2. Comparison of the values obtained by CR integration circuit and by numerical integration

Figure 5 shows the pulse shape of the digital values of magnetic flux density measurements displayed on a PC monitor. Peak magnetic flux density can be measured as the amplitude from baseline to peak of the wave.

Figure 6 shows a comparison of the magnetic flux density amplitudes measured by the CR integration circuit and those obtained by numerical integration of induced V, using the same search coil placed at the center of a circular coil with a diameter of 100 mm, as the applied voltage was changed from 400 to 2000 V.

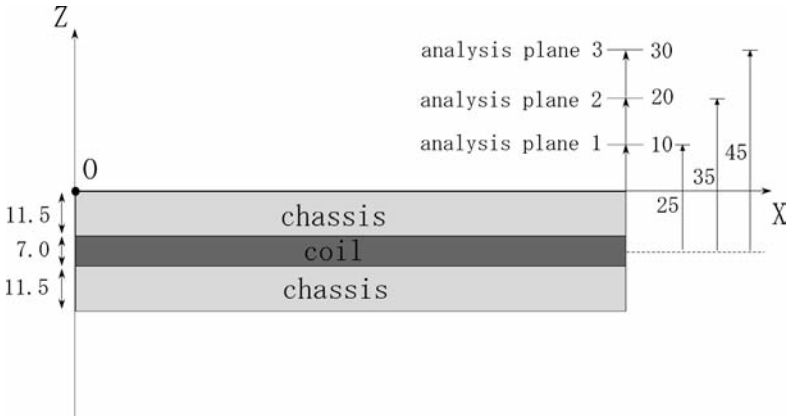

Figure 4. Lateral view of one wing of the FOE coil and analysis planes for the magnetic flux density.
Numbers indicate length (mm). Magnetic flux density was calculated at the analysis planes 1 (z ＝10 mm), 2 (z ＝20 mm) and 3 (z ＝30 mm).

Table 1. Relationship between CR values and magnetic flux density (T) measured by CR integration circuit.

CR value (ms)	Measured magnetic flux density (T)	
	Mean	SD
0.29	0.498	0.00
0.60	0.545	9.40×10^{-4}
1.45	0.563	2.74×10^{-3}
2.88	0.581	1.10×10^{-3}
4.15	0.585	1.34×10^{-3}
5.99	0.589	4.15×10^{-3}
11.58	0.578	4.51×10^{-3}
21.36	0.654	5.00×10^{-3}

C, capacitance (9.705 μF); R, resistance (30–2201 Ω); SD, standard deviation

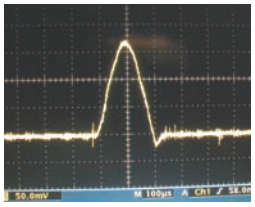

Figure 5. A computer monitor image of a CR-integrated result.
The horizontal axis indicates time with divisions of 0.1 ms, and the vertical axis indicates magnetic flux density with divisions of 0.1 T. Peak magnetic flux density can be measured as the amplitude from baseline to peak of the wave.

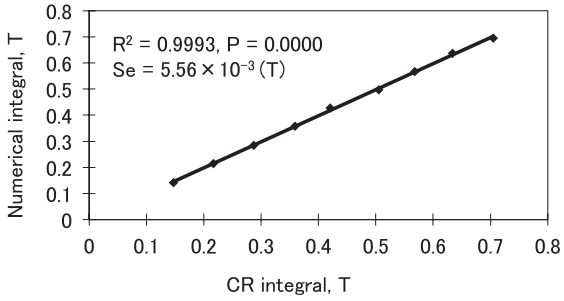

Figure 6. Comparison of magnetic flux densities measured by the CR integration circuit (horizontal axis) and the values obtained by numerical integration (vertical axis) using the same search coil with a pulse width of 0.2 ms.
R, correlation coefficient; Se, standard error.

The pulse width was kept constant at 0.2 ms throughout the measurements. The values obtained by CR integration circuit and numerical integration agreed well ($R^2=0.9993$; $P=0.0000$; standard error $=5.56\times10^{-3}$ T). Similar good agreement was obtained for magnetic flux densities from 0.1 to 1.4 T and pulse widths from 0.1 to 0.6 ms (Table 2).

3. Magnetic flux density measured by CR integration circuit

The distribution of the horizontal and vertical magnetic flux densities near the FOE coil is shown in Fig. 7. There were two peaks for the horizontal magnetic flux density (B_x). The highest peak was over the center of the coil. At 100% output, B_x at the three measured planes (z =10, 20 and 30 mm) were 0.44, 0.37, and 0.22 T, respectively. At 50% output, B_x at z

Table 2. Comparison of magnetic flux densities measured by CR integration circuit and calculated by numerical integration, using the same search coil at various turns of the coil for different pulse widths and applied voltages.

Number of turns	Applied voltage (V)	Pulse width (ms)	Output voltage (mV)	Magnetic flux density (T)	
				By CR integration circuit	By numerical integration
1	2000	0.118	7.7	0.14	0.13
2	1500	0.115	11.5	0.19	0.20
8	1000	0.126	84	1.43	1.43
12	1000	0.237	29	0.51	0.49
20	1000	0.601	13	0.22	0.22
20	2000	0.613	26	0.44	0.44

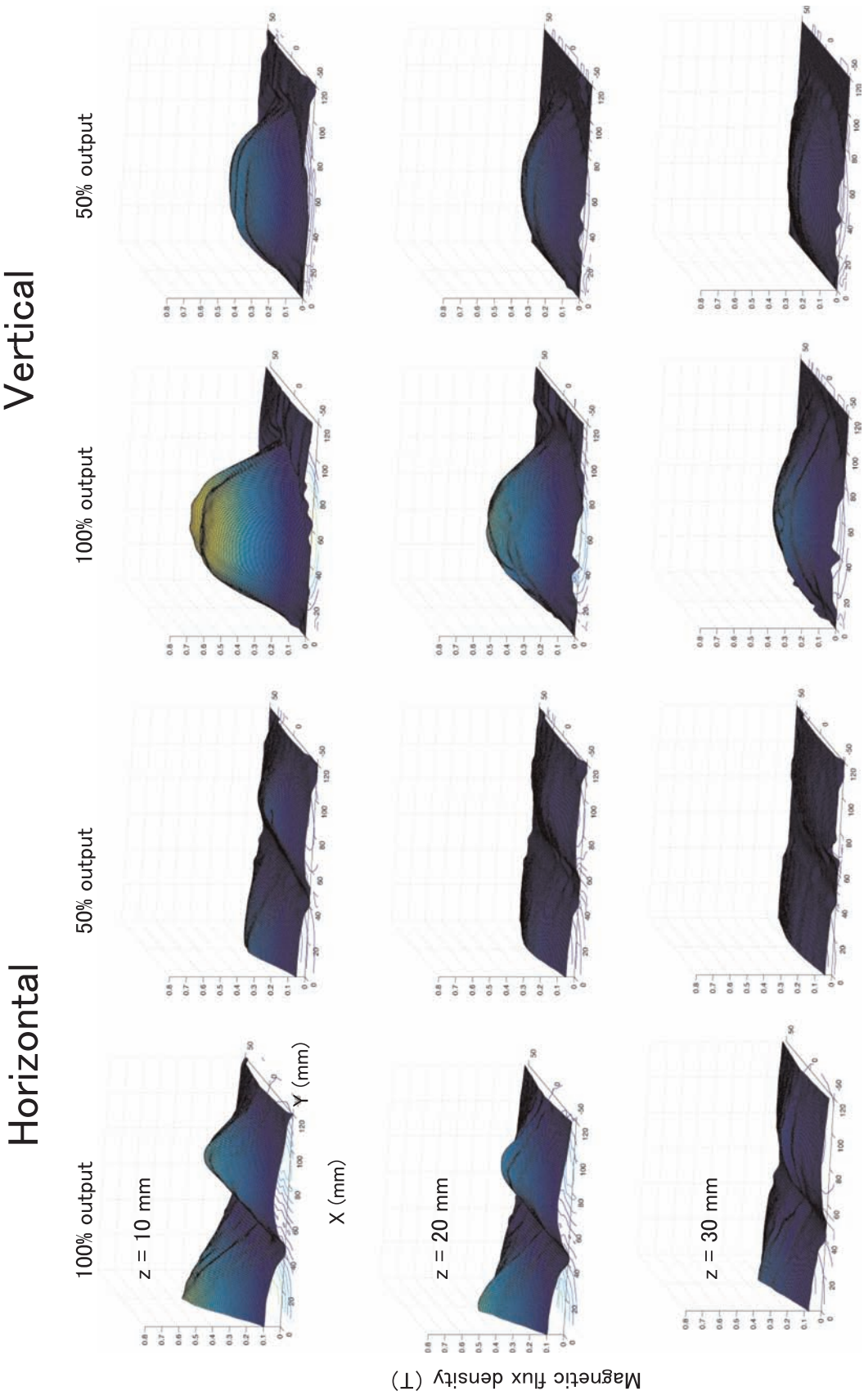

Figure 7. Distribution of the magnetic flux density around a figure-of-eight coil. Horizontal element (B_x) and vertical element (B_z) at 100% and 50% output are shown for each measurement plane ($z = 10$, 20 and 30 mm).
There are two peaks for B_x; the higher peak is over the center of the coil. B_z has one peak around the center of the circular wing of the coil. The magnetic flux density is higher at higher stimulation intensity, and lower at more distant sites from the coil.

=10, 20 and 30 mm were 0.21, 0.14 and 0.09 T, respectively. The second peak was over the outer rim of the coil. At 100% output, B_x at z =10, 20 and 30 mm were 0.36, 0.29 and 0.14 T, respectively. At 50% output, at z =10, 20 and 30 mm were 0.17, 0.10 and 0.07 T, respectively.

There was a peak for the vertical magnetic flux density (B_z), located around the center of the circular wing of the coil. At 100% output, B_z at z =10, 20 and 30 mm were 0.52, 0.38 and 0.23 T, respectively. At 50% output, B_z at z =10, 20 and 30 mm were 0.28, 0.19 and 0.18 T, respectively.

4. Magnetic flux density calculated by the FOE coil model

The theoretical values of the magnetic flux density in the FOE coil were compared with the actual measurements at 100% output power, for the transverse component B_x along three representative test lines (y =0; z =10, 20, and 30 mm). The results are shown in Fig. 8. The calculated magnetic flux densities were approximately 1.8 times larger than the experimental values, but both results showed similar behaviors overall. As was expected from equation (8), B_x had a peak at the center of the FOE coil, and showed secondary peaks at the edges of the FOE coil. The ratios of B_x at the center to B_x at the edge in the model were estimated to be 1.7, 2.1 and 2.5 at the heights of z =10, 20 and 30 mm, respectively. These values were slightly larger than the measured values of 1.2, 1.3 and 1.6, respectively.

Discussion

We developed a search coil with a CR integration circuit for instantaneous measurement of pulsed magnetic fields, and confirmed the accuracy of the measurements by comparing the data obtained from the CR integration circuit with the values obtained from numerical integration. Although magnetic field measurement using CR integration is not a new idea, there are no reports on the appropriate CR values to use or measured magnetic flux densities generated by the FOE coil commonly used in clinical laboratories, probably because of the difficulties in manufacturing such measurement devices. One of the difficulties is the selection of optimal capacitance and resistance. The capacitance displayed on a capacitor is measured using direct current and includes errors. Furthermore, it varies depending on current frequency. Thus the optimal combination of capacitance and resistance in CR circuits to measure pulsed magnetic flux densities have never been clarified. We selected CR=4 ms which proved to be appropriate for the measurement of magnetic field intensities ranging from 0.1 to 1.4 T with pulse widths ranging from 0.1 to 0.6 ms.

We report for the first time the distribution of magnetic flux densities generated by a FOE coil, which we measured using the CR integration circuit that we designed. For clinical application of TMS, it is essential to know the quality of the stimulators used in individual laboratories. Currently, the available specifications for such devices are limited to maximal *dB*/*dt* and theoretical electric fields adjacent to the coil. Thus, the data presented in this study of actual magnetic flux densities measured at a distance of 1 to

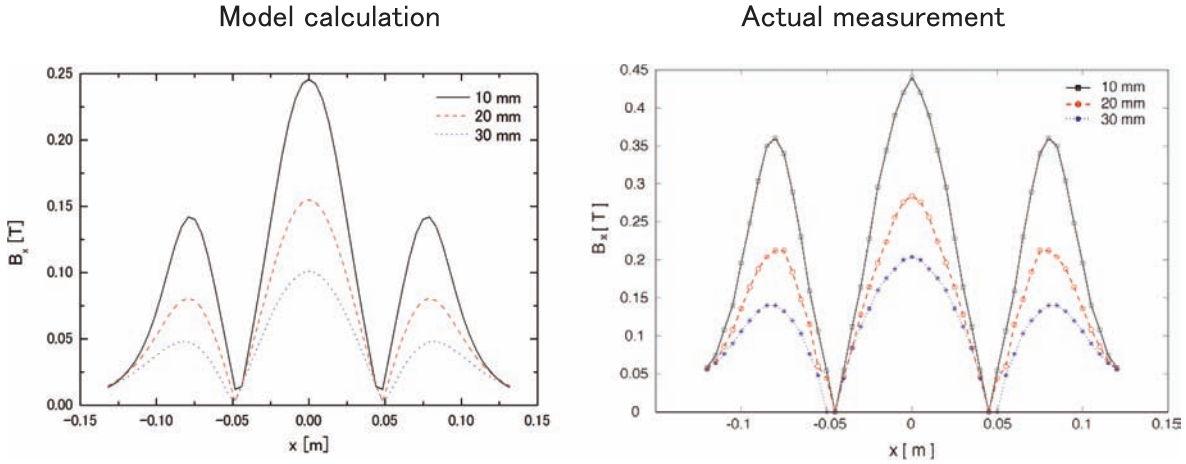

Figure 8. Comparison of magnetic flux density parallel to the x-axis (B_x) between the model calculation and actual measurements at 100% output.
Data show B_x along the lines y =0 and z =10, 20 and 30 mm. In the graph of actual measurements, values of B_x (x < 0) are plotted as mirror images of B_x (x > 0). Calculated values and experimental ones are similar. The ratio of B_x at the center (maximum peaks) to B_x at the edge (secondary peaks) in the model was estimated to be 1.7, 2.1, 2.5 at the height of z =10, 20, 30 mm, respectively. These quantities were slightly larger than the measured values of 1.2, 1.3, 1.6, respectively.

3 cm from the FOE coil surface at different stimulator outputs should be useful in quantitative analysis of the effects of TMS on cortical function, irrespective of the type of TMS device.

The motor threshold of TMS is given in individual stimulators as relative values, and absolute values are not available. Okita and Takagi [17] studied the relation between magnetic field structure and distribution of induced electric current based on a cylindrical model composed of a uniform electrically conductive medium. By choosing representative parameters of conductivity ($\delta = 0.2$S/m), frequency ($\omega = 2\pi \times 10^3$ Hz) and scale of the medium (radius = 10 cm) often used in TMS, they showed that the threshold of pulsed magnetic flux density for exciting motor nerve fibers was in the range of 0.3 to 0.8 T, which is reasonably consistent with the values reported by Izumi et al. [18]. Izumi et al. [18] found that the threshold values for activating the ulnar motor nerve at the elbow of a healthy subject ranged between 0.15 and 0.2 T at pulse widths of 0.1 to 0.4 ms. Since the motor threshold in healthy humans usually lies in the range of 50 to 100% output of the TMS device used in the present study, peak B_x amplitudes obtained from the present measurements suggest that the threshold of magnetic flux density in the human motor cortex is comparable to the threshold reported for motor nerve fibers.

A previous study that calculated the electric field near the surface of the FOE coil showed that the induced current flow is the strongest at the center of the coil, and is directed along the axis parallel to the coil handle, corresponding to the y-axis in the present study [15]. Thus, we compared the actual measurements and the model calculations of B_x which determines E_y (induced electric field parallel to the y-axis).

Good agreement was observed between the model calculations and the actual measurements of B_x. In principle, the strength of the magnetic flux density is proportional to the electric current of the coil, which is assumed to be $I_0^{\pm} = 3$ kA according to the specification of the device. The differences between the theoretical and experimental values of B_x probably originated from this assumption. However, peak B_x amplitude at the coil center relative to that at the coil edge was smaller for the actual measurements than for the model calculations, suggesting less focalization of stimulation in the actual coil than in the model. This is probably because the model calculation assumes that the two loop currents touch each other at the center, while they do not in the actual coil [15].

Future studies should examine the relationship between coil geometry and the actual magnetic flux density as well as the induced electric current estimated from a medium model, in order to create an optimal coil design for TMS to be used in patients with various central nervous system disorders.

Acknowledgement

This research was supported by the Program for Promotion of Fundamental Studies in Health Sciences of the National Institute of Biomedical Innovation, NIBIO for fiscal year 2006–2008 (Project ID 06–32).

References

1. Barker AT, Jalinous R, Freeston IL. Non-invasive magnetic stimulation of human motor cortex. Lancet 1985; 1: 1106–7.
2. Epstein CM, Schwartberg DG, Davey KR, Sudderth DB. Localizing the site of magnetic brain stimulation in humans. Neurology 1990; 40: 666–70.
3. Fregni F, Boggio PS, Valle AC, Rocha RR, Duarte J, Ferreira MJL, et al. A sham-controlled trial of a 5–day course of repetitive transcranial magnetic stimulation of the unaffected hemisphere in stroke patients. Stroke 2006; 37: 2115–22.
4. Izumi S, Kondo T, Shindo K. Transcranial magnetic stimulation synchronized with maximal movement effort of the hemiplegic hand after stroke: a double-blinded controlled pilot study. J Rehabil Med 2008; 40: 49–54.
5. Kim Y-H, You SH, Ko M-H, Park Ji-W, Lee KH, Jang SH, et al. Repetitive transcranial magnetic stimulation-induced corticomotor excitability and associated motor skill acquisition in chronic stroke. Stroke 2006; 37: 1471–6.
6. Mansur CG, Fregni F, Boggio PS, Riberto M, Gallucci-Neto J, Santos CM, et al. A sham stimulation controlled trial of rTMS of the unaffected hemisphere in stroke patients. Neurology 2005; 64: 1802–4.
7. Takeuchi N, Chuma T, Matsuo Y, Watanabe I, Ikoma K. Repetitive transcranial magnetic stimulation of contralesional primary motor cortex improves hand function after stroke. Stroke 2005; 36: 2681–6.
8. Brighina F, Bisiach E, Oliveri M, Piazza A, La Bua V, Daniele O, et al. 1 Hz repetitive transcranial magnetic stimulation of the unaffected hemisphere ameliorates contralesional visuospatial neglect in humans. Neurosci Lett 2003; 336: 131–3.
9. Devlin JT & Watkins KE. Stimulating language: insights from TMS. Brain 2007; 130: 610–22.
10. Naeser MA, Martin PI, Treglia E, Ho M, Kaplan E, Bashir S, et al. Research with rTMS in the treatment of aphasia. Restor Neurol Neurosci 2010; 28: 511–29.
11. Shindo K, Sugiyama K, Huabao Lu, Nishijima K, Kondo T, Izumi S. Long-term effect of low-frequency repetitive transcranial magnetic stimulation over the unaffected posterior parietal cortex in patients with unilateral spatial neglect. J Rehabil Med 2006; 38: 65–7.
12. Ueno S, Tashiro T, Harada K. Localized stimulation of neural tissue in the brain by means of a paired configuration of time-varying magnetic fields. J Appl Physics 1988; 64: 5862–4.
13. Hallett M. Transcranial magnetic stimulation and the human brain. Nature 2000; 406: 147–50.
14. Thielscher A & Kammer T. Electric field properties of

two commercial figure−8 coils in TMS: calculation of focality and efficiency. Clin Neurophysiol 2004; 115: 1697−708.
15. Thielscher A & Kammer T. Linking physics with physiology in TMS: A sphere field model to determine the cortical stimulation site in TMS. Neuroimage 2002; 17: 1117−30.
16. Jackson JD. Classical Electrodynamics. John Wiley & Sons, New York, 1975.
17. Okita T & Takagi T: Magnetic field structure and induced electric current distribution on a cylindrical model: Application to magnetic nerve stimulation. Chin Phys Lett 2009; 26: 074101−1−4.
18. Izumi S, Takagi T, Nagatomi R, Nakasato N, Yashima Y, Abe T. Fabrication of multi-coil system for deep brain transcranial magnetic stimulation. Jpn J Clin Neurophysol 2009; 37: 1−9.